Magnetorotational and Parker instabilities in magnetized plasma Dean flow as applied to centrifugally confined plasmas

Yi-Min Huang[a)] and A. B. Hassam[b)]
Institute for Research in Electronics and Applied Physics, University of Maryland, College Park, Maryland 20742

(Received 29 August 2002; accepted 22 October 2002)

The ideal magnetohydrodynamics stability of a Dean flow plasma supported against centrifugal forces by an axial magnetic field is studied. Only axisymmetric perturbations are allowed for simplicity. Two distinct but coupled destabilization mechanisms are present: flow shear (magnetorotational instability) and magnetic buoyancy (Parker instability). It is shown that the flow shear alone is likely insufficient to destabilize the plasma, but the magnetic buoyancy instability could occur. For a high Mach number (M_S), high Alfvén Mach number (M_A) system with $M_S M_A \gtrsim \pi R/a$ (R/a is the aspect ratio), the Parker instability is unstable for long axial wavelength modes. Implications for the centrifugal confinement approach to magnetic fusion are also discussed.
 [DOI: 10.1063/1.1528937]

I. INTRODUCTION

An idea currently under investigation is to use the centrifugal force of a rotating plasma to augment magnetic confinement for thermonuclear fusion plasmas.[1] In this scheme, a magnetic mirror type plasma is made to rotate azimuthally at supersonic speeds; thus, centrifugal forces confine the plasma to the central section. The central issue here is the ideal MHD (magnetohydrodynamics) stability of the system. Previous studies indicate that the prevalent interchange mode can be stabilized by the strong velocity shear that accompanies the rotation.[2,3] However, all the previous studies are based on the ordering $C_S \lesssim u \ll V_A$, where C_S is the sound speed, u is the flow speed, and V_A is the Alfvén speed. In that case, the strong magnetic field stabilizes any fluctuation along the field, and the calculations were done for nonaxisymmetric flute modes. From the fusion viewpoint, however, the output power is proportional to the square of the particle density; for a device with a given magnetic field, a high β ($\equiv 2p/B^2 \sim C_S^2/V_A^2$) system with $u \sim V_A$ is highly desirable. For such a system, the magnetic field may not be strong enough to stabilize fluctuations along the field. Thus, ideal MHD instabilities with axial wave numbers need investigation.

An immediate concern is the magnetorotational instability (MRI).[4–7] Since the recent work by Balbus and Hawley,[6] the MRI has attracted broad attention and is believed to be the cause of the turbulent angular momentum transport in accretion disks. Roughly speaking, the stability criterion based on a local analysis is[7]

$$(\mathbf{k}\cdot\mathbf{V}_A)^2 > -\frac{d\Omega^2}{d\ln(r)}, \tag{1}$$

where $\mathbf{k}$ is the wave number and Ω is the angular frequency. Condition (1) can only be violated where $\partial_r \Omega^2 < 0$, which is usually true for most astrophysical disks. In a centrifugally confined plasma, a parabola-like Ω profile is expected,[2,3] hence the MRI is possible in the outboard half of the system. Condition (1) also indicates that a system with high Alfvén Mach number ($M_A \sim r\Omega/V_A$) and high elongation (which allows smaller k) is more prone to the MRI. Since both attributes are desirable for centrifugal confinement schemes (high M_A means high β, and elongation assists velocity shear stabilization, see Ref. 8), whether or not the MRI is a fundamental limit needs more investigation.

Another possible destabilizing mechanism is magnetic buoyancy. It was first pointed out by Parker[9] that a magnetized plasma partially supported against gravity by a magnetic field could be unstable. When the Parker instability occurs, the plasma in a flux tube spontaneously fragments into clumps, which are then pulled "downward" by the gravity. Meanwhile, the dilute parts of the flux tube bulge upward, in a way that resembles a buoyant light bubble in a heavy fluid. Parker suggested this as an explanation for the nonuniformity of the interstellar medium inside a galaxy. Although there is no gravity in the centrifugal confinement scheme, the plasma is supported by the magnetic field against the centrifugal force, which plays the role of the gravity. It was pointed out in Ref. 10 that for rotating stellar winds or accretion disks in which the magnetic pressure of nonuniform poloidal magnetic fields balance the combination of gravity and centrifugal forces, a poloidal buoyancy mode resembling the Parker instability could occur. The same instability would also be an issue for the centrifugal confinement scheme.

In this paper, we study the above-mentioned issues in more detail. To avoid the complication of the curved-field geometry of the centrifugal confinement scheme, we model the system with the straight-field Dean flow model, as we did in our previous study.[2] The effect of a curved field, though not fully understood at present, will be briefly assessed later.

a)Electronic mail: yopology@umd.edu
b)Electronic mail: hassam@umd.edu

It is worth pointing out that although the MRI and the magnetic buoyancy instability involve different mechanisms, they are inextricably coupled, and there is no way to clearly distinguish one from the other.

This paper is organized as follows. In Sec. II, we set up the Dean flow model and the governing equations. In Sec. III, we first linearize the equations about the equilibrium, then numerically solve the eigenvalue equation so obtained by a shooting code. Before solving the general equation, two simple limiting cases, the cold plasma limit and the incompressible limit, are considered. In Sec. IV, we confirm the results of Sec. III by a series of initial value simulations. In Sec. V, We discuss the implications for centrifugally confined plasmas. We conclude in Sec. VI.

II. THE DEAN FLOW MODEL

For simplicity, we consider only the axisymmetric case. In the cylindrical coordinate system (r,ϕ,z), the most general divergence-free magnetic field can then be written as

$$\mathbf{B}=I\nabla\phi+\nabla\phi\times\nabla\psi\equiv B_\phi\hat{\phi}+\mathbf{B}_\perp . \tag{2}$$

We decompose the flow velocity into the azimuthal component and the perpendicular component: $\mathbf{u}=u_\phi\hat{\phi}+\mathbf{u}_\perp$. The ideal MHD equations with an adiabatic equation of state (for $\partial/\partial\phi=0$) are

$$\frac{d\rho}{dt}=-\rho\nabla\cdot\mathbf{u}_\perp , \tag{3}$$

$$\rho\frac{d\mathbf{u}_\perp}{dt}=-\frac{\nabla_\perp I^2}{2r^2}-\frac{\nabla_\perp\psi}{r^2}\left(\nabla^2\psi-2\frac{\partial_r\psi}{r}\right)+\rho\frac{u_\phi^2}{r}\hat{r}-\nabla_\perp p, \tag{4}$$

$$\rho\frac{du_\phi}{dt}=\frac{\mathbf{B}_\perp\cdot\nabla_\perp I}{r}-\rho\frac{u_\phi u_r}{r}, \tag{5}$$

$$\frac{dI}{dt}=r^2\mathbf{B}_\perp\cdot\nabla_\perp\left(\frac{u_\phi}{r}\right)-Ir^2\nabla\cdot\left(\frac{u_2}{r^2}\right), \tag{6}$$

$$\frac{d\psi}{dt}=0, \tag{7}$$

$$\frac{dp}{dt}=-\gamma p\nabla\cdot\mathbf{u}_\perp, \tag{8}$$

where

$$\frac{d}{dt}\equiv\frac{\partial}{\partial t}+\mathbf{u}_\perp\cdot\nabla_\perp , \tag{9}$$

$$\nabla_\perp\equiv\hat{r}\partial_r+\hat{z}\partial_z . \tag{10}$$

Standard notation is used. ρ is the plasma density, p is the pressure, and γ is the adiabatic index.

Figure 1 depicts the Dean flow model we used. The plasma is contained in an annular box with inner radius R, box width a, and elongation L. We assume the following equilibrium: $p=$const, $\rho=$const, $\mathbf{B}=B(r)\hat{z}=-(1/r)\partial_r\psi\hat{z}$, and $\mathbf{u}=r\Omega(r)\hat{\phi}$. The centrifugal force is balanced by the magnetic force:

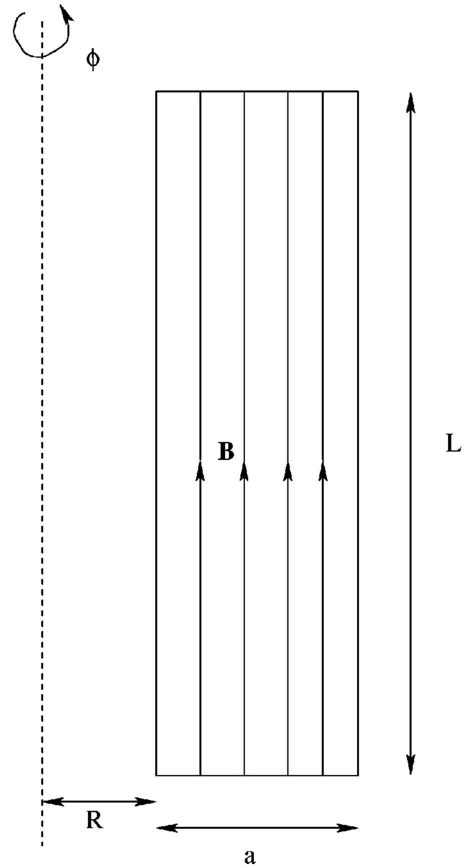

FIG. 1. A Dean flow model for the straight section of a centrifugally confined plasma. A plasma within an annular box with inner radius R, width a, and elongation L is threaded by a straight magnetic field in $\hat{z}$.

$$\rho r\Omega^2=B\partial_r B=\frac{\partial_r\psi}{r^2}\left(\partial_r^2\psi-\frac{\partial_r\psi}{r}\right). \tag{11}$$

The assumed flat density profile and pressure profile may seem special. To be sure, the gradient of those profiles will affect the stability criteria. However, this model captures the essential physics: the sheared velocity profile allows MRI, and the compressibility allows a magnetic buoyancy instability. It is worth mentioning that in the centrifugal confinement scheme, a hot plasma is supported by the magnetic field against both the centrifugal force and the pressure gradient; for optimum confinement, a sonic Mach number of $M_S=4-5$ is desired, which is to say that the centrifugal force dominates the pressure gradient provided the aspect ratio $R/a\ll M_S^2\sim 20$. If the system has such a large aspect ratio ($\sim$20, which is unlikely), we can no longer neglect the pressure gradient in force balance, and accordingly the constant pressure assumption is not appropriate.

III. LINEAR STABILITY ANALYSIS

A. Derivation of the eigenvalue equation

We now linearize (3)–(8) about the above-mentioned equilibrium. We assume perturbations of the form $\rho\rightarrow\rho(r)+\tilde{\rho}(r)\exp(ik_z z-i\omega t)$, etc. The resulting linearized equations are

$$-i\omega\tilde{\rho}=-\rho\left(\tilde{u}_r'+ik_z\tilde{u}_z+\frac{\tilde{u}_r}{r}\right), \tag{12}$$

$$-i\omega\rho\tilde{u}_r=\frac{B}{r}\left(\tilde{\psi}''-k_z^2\tilde{\psi}-\frac{\tilde{\psi}'}{r}\right)+\frac{\rho\Omega^2}{B}\tilde{\psi}'+2\rho\Omega\tilde{u}_\phi$$
$$+\tilde{\rho}r\Omega^2-\tilde{p}', \tag{13}$$

$$-\omega\rho\tilde{u}_z=\frac{\rho\Omega^2}{B}k_z\tilde{\psi}-k_z\tilde{p}, \tag{14}$$

$$-i\omega\rho\tilde{u}_\phi=ik_z\frac{B}{r}\tilde{I}-2\rho\Omega\tilde{u}_r-\rho r\Omega'\tilde{u}_r, \tag{15}$$

$$-\omega\tilde{I}=k_z r\Omega'\tilde{\psi}+k_z rB\tilde{u}_\phi, \tag{16}$$

$$-i\omega\tilde{\psi}=rB\tilde{u}_r, \tag{17}$$

$$-i\omega\tilde{p}=-\gamma p\left(\tilde{u}_r'+ik_z\tilde{u}_z+\frac{\tilde{u}_r}{r}\right), \tag{18}$$

where primes denote differentiation with respect to r. Eliminating $\tilde{u}_z$, $\tilde{u}_\phi$, $\tilde{\rho}$, $\tilde{p}$, $\tilde{\psi}$, and $\tilde{I}$ from Eqs. (12) to (18), after some algebra, we obtain the following eigenvalue equation for $\tilde{u}_r$:

$$(\omega^2-k_z^2V_A^2)\left(F\tilde{u}_r''+\frac{(rF)'}{r}\tilde{u}_r'+G\tilde{u}_r\right)$$
$$-4\omega^2\Omega^2(\omega^2-k_z^2C_S^2)\tilde{u}_r=0, \tag{19}$$

where $C_S^2\equiv\gamma p/\rho$, and $V_A^2(r)\equiv B^2(r)/\rho$ are the square of the sound speed and the Alfvén speed, respectively. The two functions $F(\omega,k_z,r)$ and $G(\omega,k_z,r)$ are defined as

$$F=(V_A^2+C_S^2)\omega^2-k_z^2V_A^2C_S^2, \tag{20}$$

$$G=\omega^4-\left(k_z^2+\frac{1}{r^2}\right)F+2\omega^2\Omega^2-2k_z^2C_S^2(\Omega^2-r\Omega\Omega')$$
$$-k_z^2r^2\Omega^4. \tag{21}$$

In deriving Eqs. (12)–(19), we use Eq. (11) repeatedly to express $B'(r)$ in terms of Ω.

We can eliminate the first-order derivative term of Eq. (19) by substituting $\tilde{u}_r=(rF)^{(-1/2)}u$. The eigenvalue equation for u is

$$(\omega^2-k_z^2V_A^2)(Fu''+Hu)-4\omega^2\Omega^2(\omega^2-k_z^2C_S^2)u=0, \tag{22}$$

where

$$H=\omega^4-\left(k_z^2+\frac{3}{4r^2}\right)F+(2k_z^2C_S^2-\omega^2)2r\Omega\Omega'$$
$$+\frac{r^2\Omega^4(\omega^2-k_z^2C_S^2)^2}{F}-k_z^2r^2\Omega^4. \tag{23}$$

We assume impenetrable hard wall boundary conditions; therefore, Eq. (22) has to be solved subject to the homogeneous boundary conditions $u(R)=u(R+a)=0$.

In this paper, we will take the parabolic angular frequency profile $\Omega=4\Omega_0(r-R)(a+R-r)/a^2$ as our basic model, which mimics what we expect in the centrifugal confinement scheme. The system is then characterized by three parameters: the Mach number $M_S\equiv(R+a/2)\Omega_0/C_S$, the Alfvén Mach number $M_A\equiv(R+a/2)\Omega_0/(V_A|_{R+a})$, and the aspect ratio R/a. We took $R/a=1/3$ for most parts of the study; the effect of the aspect ratio will be discussed briefly later. The main task of this work is to assess the stability with respect to the parameter space.

The eigenvalue equation (22) is quite complicated; numerical solutions are needed. A simple shooting code in MATHEMATICA is written for this purpose. The code allows complex eigenvalue ω^2; however, we found no solution with complex eigenvalue in this study (although we cannot prove this in general). Before tackling the general case, we will consider some limiting cases first.

B. Cold plasma limit, $C_S\to 0$

As a first limit, we assume the plasma to be cold. In the $C_S\to 0$ limit, Eq. (22) becomes

$$(\omega^2-k_z^2V_A^2)\left(\omega^2V_A^2u''+\left(\omega^4-\left(k_z^2+\frac{3}{4r^2}\right)\omega^2V_A^2\right.\right.$$
$$\left.\left.-2r\Omega\Omega'\omega^2+\frac{r^2\Omega^4\omega^2}{V_A^2}-k_z^2r^2\Omega^4\right)u\right)-4\omega^4\Omega^2u=0. \tag{24}$$

The eigenvalue ω^2 of (24) can be shown to be real (see Appendix A). In this case, ω is either real or purely imaginary, which means the transition from stable modes to unstable modes must occur through $\omega=0$. Therefore, we can look for marginal stability by letting $\omega=0$ in Eq. (24), which simply yields $k_z=0$ provided $\Omega\neq 0$. Since no marginal mode with nonzero k_z exists, either the system is stable for all k_z wave numbers, or modes of all k_z are unstable. Now consider the short wavelength modes, $k_z\gg 1/a$, $1/R$, and for the moment assume $|\omega|\ll k_zV_A$, since we are not interested in the those fast modes, which are stable. Under these approximations, Eq. (24) becomes

$$u''-k_z^2\left(1+\frac{r^2\Omega^4}{\omega^2V_A^2}\right)u=0. \tag{25}$$

Since k_z is large by assumption, for any localized solution of (25) which peaks at a certain radius r_0, we must have

$$\left(1+\frac{r^2\Omega^4}{\omega^2V_A^2}\right)_{r_0}\simeq 0; \tag{26}$$

otherwise the second term on the left-hand side of Eq. (25) will be very large. Equation (26) gives the local dispersion relation $\omega^2\simeq -r^2\Omega^4/V_A^2$, which corresponds to unstable modes with growth rate $\simeq r\Omega^2/V_A$. This is the well-known local Parker instability growth rate (see Refs. 9 and 10, also Appendix B), with the centrifugal acceleration $r\Omega^2$ replacing the gravity in astrophysical systems. In this limit, the major destablization mechanism comes from the centrifugal force, and the differential rotation Ω' is less important. The self-consistency condition $|\omega|\ll k_zV_A$ requires $r\Omega^2\ll k_zV_A^2$, which can be easily satisfied with k_z large enough. The above local dispersion relation is confirmed for the basic model by numerical solutions with large k_z.

We have proved that short wavelength modes are unstable provided $\Omega \neq 0$. From our previous marginal mode argument, we have actually proved the system to be unstable for all k_z wave numbers. The reason for this is not difficult to understand. If the plasma is cold, we can always compress the plasma along the field without consuming any work; that means we can build up a local high density region simply by compression—with no cost. One can make the local density as high as needed until the magnetic tension can no longer stop the centrifugal force from pulling it outward, Likewise, the low density part will be pushing inward due to the excess of the magnetic pressure. As we will see, including the plasma temperature, thus restoring the sound wave, stabilizes the Parker instability, especially for short wavelength modes.

C. Incompressible limit, $C_S \to \infty$

We next consider the incompressible limit. In this limit, the system cannot have the magnetic buoyancy instability and MRI is the only mechanism of destabilization. Since the centrifugal confinement scheme, as we mentioned, requires high M_S, this limit may not be realistic. However, this limit can help us elucidate why the MRI is likely not an issue in the centrifugal confinement scheme. In the $C_S \to \infty$ limit, Eq. (22) becomes

$$(\omega^2 - k_z^2 V_A^2)^2 u'' + \left(-\left(k_z^2 + \frac{3}{4r^2} \right)(\omega^2 - k_z^2 V_A^2)^2 + 4k_z^2(\omega^2 - k_z^2 V_A^2) r\Omega\Omega' + k_z^4 r^2 \Omega^4 + 4\omega^2 k_z^2 \Omega^2 \right) u = 0. \tag{27}$$

For various M_A and R/a we have tried, no unstable mode was found for the basic model. This is confirmed by the result of the general case that the system is always stable when M_S is smaller than some critical value (see Sec. III D), and direct simulations of the next section). In order to gain some understanding of this fact, we consider the local Wertzel–Kramers–Brillouin (WKB) dispersion relation as follows. It should be mentioned that the validity of the WKB dispersion relation for this kind of problem is questionable; nevertheless, previous studies show that it agrees with the global result to a certain extent, therefore it can be used as a reasonable stability criteria (see, for example, Ref. 11). By letting $\partial_r^2 \to -k_r^2$ in Eq. (27), the WKB dispersion relation is

$$\left(k^2 + \frac{3}{4r^2} \right) \omega^4 - 2k_z^2 \left(V_A^2 \left(k^2 + \frac{3}{4r^2} \right) + 2(\Omega^2 + r\Omega\Omega') \right) \omega^2 + k_z^4 \left(\left(k^2 + \frac{3}{4r^2} \right) V_A^4 + 4V_A^2 r\Omega\Omega' - r^2\Omega^4 \right) = 0, \tag{28}$$

with $k^2 \equiv k_r^2 + k_z^2$. Equation (28) is quadratic in ω^2, and it is easy to show that the determinant is positive, hence ω^2 is real. To have unstable modes, i.e., $\omega^2 < 0$, the coefficient of ω^0 has to be negative, or

$$\left(k^2 + \frac{3}{4r^2} \right) V_A^4 < -4V_A^2 r\Omega\Omega' + r^2\Omega^4. \tag{29}$$

Equation (29) indicates the key characteristic of the MRI—the flow shear is destabilizing only when $\Omega' < 0$. For the parabolic Ω profile we assumed, only the outboard half of the system could be unstable. Equation (29) also indicates that a system with a larger angular frequency and a weaker magnetic field is more likely to be unstable. However, the force balance condition (11) relates the magnetic field strength to the angular frequency—they are no longer independent. This fact makes the centrifugal confinement device quite different from the accretion disk[7] and the proposed MRI experiment of liquid metal,[11] where the centrifugal force is mostly balanced by gravity in the former (Keplerian flow) and pressure gradient in the later. In those cases the magnetic field could be arbitrarily weak, that makes the systems more prone to the MRI. Now we do a simple dimensional analysis. Roughly speaking, in the outboard half, $V_A^2 \sim ar\Omega^2$ from Eq. (11), and $\Omega' \sim -\Omega/a$. The minimum total wave number k is limited by the longest wavelength allowed by the system size, hence $k \gtrsim \pi/a$. Substituting all these into (29), we can see the instability criterion is not satisfied. Although this is a very crude estimate, it indicates that the MRI is likely not an issue for the centrifugal confinement scheme. The reason for that is simple: for a system with parabola-like angular frequency, the MRI is only possible in the outboard half, where the magnetic field is strong enough to stabilize the MRI. One might think that for a system in which the angular frequency decreases all the way outward, e.g., the Couette flow, the MRI could be possible. This is certainly true. In some cases of the Couette flow, we have found localized unstable modes about the inner wall, where the magnetic field is weak. However, for most cases this is not even possible, as the magnetic field strength increases so quickly with the radius r that no unstable mode can be found.

D. Stability over the parameter range

We now numerically solve the system in the general case by the shooting code. The code found no unstable modes for low M_S systems, whereas for high M_S systems unstable modes were found in the region of large M_A and small k_z. Figure 2 shows the contour plot of the growth rates of the most unstable mode for the case $M_S = 4$ in the parameter space of M_A and the normalized wave number $k_z a$. The system is more unstable for high M_A since the magnetic field is weaker, and is stable for short wavelengths because of the strong magnetic recovering force at short wavelengths. It is also important to see how the unstable parameter range varies with respect to different M_S. This can be done by solving the marginal stability for different M_S. Since the ω^2 of the unstable modes we found are real, we can solve for marginal stability by setting ω^2 to zero in Eq. (22), which gives (assume $k_z \neq 0$)

$$u'' - \left(k_z^2 + \frac{3}{4r^2} + \frac{4r\Omega\Omega'}{V_A^2} - \frac{r^2\Omega^4}{V_A^4} - \frac{r^2\Omega^4}{V_A^2 C_S^2} \right) u = 0. \tag{30}$$

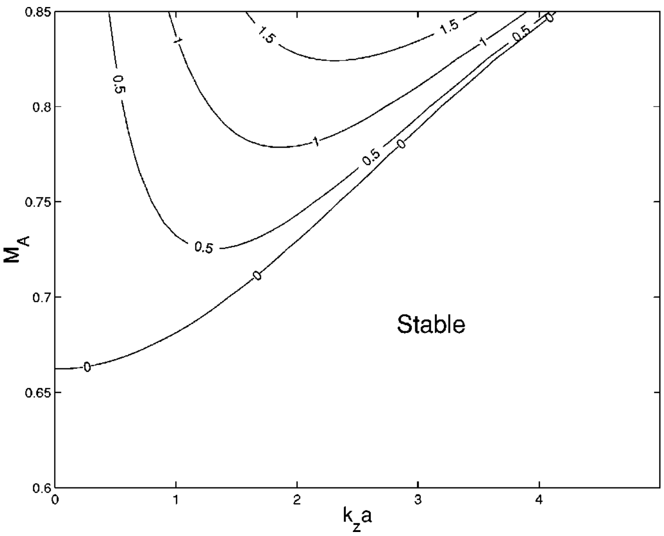

FIG. 2. Normalized growth rates of the most unstable modes for the case $M_S = 4$, $R/a = 1/3$. The growth rate is normalized to the inverse of the sound time scale, C_S/a.

Equation (30) is a Schrödinger-type eigenvalue equation of u with eigenvalue k_z^2. If Eq. (30) has no positive eigenvalue k_z^2, then the system is stable. Before we solve it numerically, a general observation can be made as follows. If we let $r \rightarrow R$, $\Omega' \rightarrow -\Omega/a$ in (30), and notice that $u'' \sim -(\pi/a)^2 u$ for a solution with the longest wavelength in the r direction, we have the schematic stability criterion:

$$-\frac{\pi^2}{a^2} - \frac{3}{4R^2} + \frac{4M_{\mathrm{A}}^2}{Ra} + \frac{M_{\mathrm{A}}^4}{R^2} + \frac{M_{\mathrm{A}}^2 M_S^2}{R^2} < 0. \tag{31}$$

The last term of the left-hand side of Eq. (31) is the only one related to M_S. Since that term is positive and proportional to M_S^2, a system with higher M_S is more unstable. This is consistent with our previous results that the system is unstable for all M_{A} and k_z in the cold limit ($M_S \rightarrow \infty$) and is completely stable in the incompressible limit ($M_S \rightarrow 0$). Figure 3

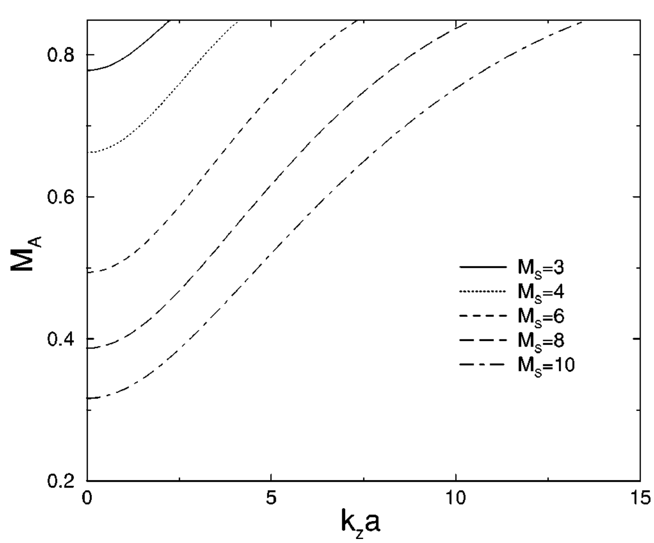

FIG. 3. Marginal stability curves for $M_S = 3,4,6,8,10$, with $R/a = 1/3$. The region above the curve is unstable.

depicts the marginal stability curves for different M_S, which clearly shows the enlargement of the unstable region as M_S increases.

IV. INITIAL VALUE SIMULATION

So far our conclusions were obtained by solving the linearized normal mode equation by the shooting code. However, it should be kept in mind that the normal modes could be incomplete, and some normal modes might even be difficult to find by a shooting code, especially those solutions involving cancellation of large terms in the equation. Even without the above-mentioned problems, one still cannot expect to obtain a complete answer by a shooting code. A shooting code can find some normal modes, but certainly not all—usually for a given k_z there exists infinite number of normal modes. Therefore, it is desirable to check the result by direct simulation.

For this purpose, we solved the time-dependent two-dimensional MHD equations for our basic model. The code we used is nonlinear although for this work we are only interested in linear stability. The numerical algorithm is described in detail in Ref. 12. The code has viscosity and resistivity explicitly. In addition to those physical transports, it also has hyperviscosity (proportional to Δx^3, where Δx is the grid size) for numerical stability. In order to have an ideal MHD equilibrium, the steady state is "frozen-in" (otherwise resistivity will flatten the magnetic field profile and viscosity will slow down the flow) and the code steps only the deviation from the steady state; therefore the nonideal effect of the code is limited to those perturbed quantities. Periodic boundary conditions are assumed in the z direction, which quantize the allowable wave numbers in the z axis. The steady state was initially seeded with a random perturbation of the size $10^{-4} C_S$ in u_r, u_ϕ, and u_z to see if the system goes unstable in time evolution. We wish to confirm (1) that the mode growth rate obtained by the shooting code agrees with the direct simulation in the linear stage, and (2) that the system is indeed stable in the parameter range where no unstable modes were found. To calculate the growth rate for each wave number from the simulation data, first we perform Fourier transformation on u_r to obtain the amplitude of each wavelength as a function of r:

$$A(k_z, r) = \int_0^L u_r(r,z) \exp(i k_z z) dz, \tag{32}$$

then average the log of the norm of $A(k_z, r)$ over radius:

$$\langle \ln|A| \rangle = \frac{1}{a} \int_R^{R+a} \ln|A(k_z, r)| dr. \tag{33}$$

By plotting $\langle \ln|A| \rangle$ with respect to time, one can then obtain the growth rate for each wave number by means of a least-squares fit during the linear growing period. This test has been run for various Mach numbers, Alfvén Mach numbers, elongation, and resolution. In terms of stability, the simulation results agree with the shooting code ones for all the cases we have tested, as summarized in Table I.

Figure 4 shows the time evolution of $\langle \ln|A| \rangle$ for the six longest wavelength modes in model 1a. According to linear

TABLE I. A comparison between the normal mode shooting code results and the initial value simulation results.

Model	(r,z) Grid	L/a	M_S	M_A	Shooting code	Simulation
1a	45×133	2π	6	0.75	Unstable	Unstable
1b	45×133	1.2	6	0.75	Stable	Stable
1c	45×133	1.3	6	0.75	Unstable	Unstable
1d	60×261	2π	6	0.75	Unstable	Unstable
2a	45×133	2π	6	0.6	Unstable	Unstable
2b	45×133	2	6	0.6	Stable	Stable
3a	45×133	2π	4	0.75	Unstable	Unstable
3b	45×133	2	4	0.75	Stable	Stable

analysis, $k_z a=1-5$ will be unstable. The simulation shows that $k_z a=6$ is also unstable, after $t\simeq 4$. An obvious possible reason for this is the nonlinear coupling between modes. As we can see from Fig. 4, the mode with $k_z a=1$ has two stages of ''linear growing,'' with a smaller growth rate within $t=2-5$, followed by a sudden boost at $t\simeq 5$. This sudden boost also indicates nonlinear coupling. For the same reason, although the $k_z a=5$ mode should be weakly unstable according to linear analysis, we cannot trust the ''linear growth'' of that mode shown in Fig. 4, since the behavior resembles that of $k_z a=6$. To verify the hypothesis of nonlinear coupling, we tested the model 1b, with elongation 1.2, which limits the smallest wave number to $k_z a=5.24$. According to linear analysis, this wave number will be stable, which is confirmed by the simulation. Model 1b has been run for t=30 to ensure that no slowly growing modes exist. As a comparison to model 1b, model 1c, with a slightly longer elongation 1.3, has the smallest wave number $k_z a=4.83$, which is unstable according to the linear analysis. This linear growth is clearly shown in Fig. 5.

The mode growth rates calculated from models 1a–1c are plotted in Fig. 6 and compared with the growth rate from the shooting code. We found that the growth rate from simulation agrees with the shooting code result but is slightly lower, which is clearly due to the nonideal terms in the code. To test this possibility, we have to decrease the viscosity and resistivity. This can be done in a simulation with higher resolution, which also reduces hyperviscosity. Model 1d is essentially a high resolution version of model 1a, but the resistivity and the viscosity are decreased by a factor of 2. The resulting growth rates are closer to the ones from the shooting code, as also shown in Fig. 6.

The agreement between the linear analysis and the simulation lays a solid foundation for the results obtained in the previous section. In particular, the stable region found by the shooting code is indeed so.

V. IMPLICATIONS FOR CENTRIFUGALLY CONFINED PLASMAS

As we mentioned in Sec. I, a high β system is desirable for a fusion device. Since $\beta=2p/B^2=(2/\gamma)M_A^2/M_S^2$, to achieve high β we have to achieve high M_A. As we can see from Fig. 3, for a plasma with $M_S=4$, the maximum stable $M_A\simeq 0.66$, which yields $\beta\simeq 3.3\%$ ($\gamma=5/3$ is assumed). However, the above-mentioned estimate is based on infinite elongation, which allows all possible $k_z a$ down to zero. For a system with finite elongation L, we have $k_z a \geqslant \pi a/L$, which makes the system more stable. However, elongation only slightly affects the stability. For example, the maximum stable $M_A\simeq 0.7$ when $L/a=2$, which is not much different from the infinite elongation case. Notice that while our previous study[8] shows that large elongation is desirable for velocity shear stabilization of the interchange instability, the present study indicates that a system with long elongation is

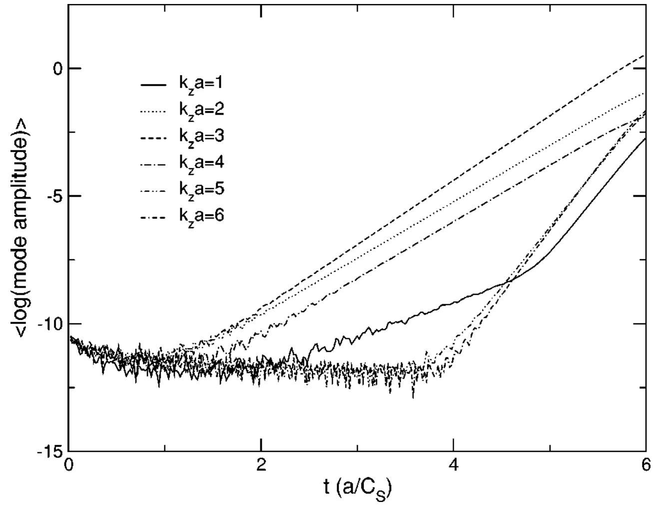

FIG. 4. Time evolution of $\langle \ln|A| \rangle$ for various wave numbers of model 1a.

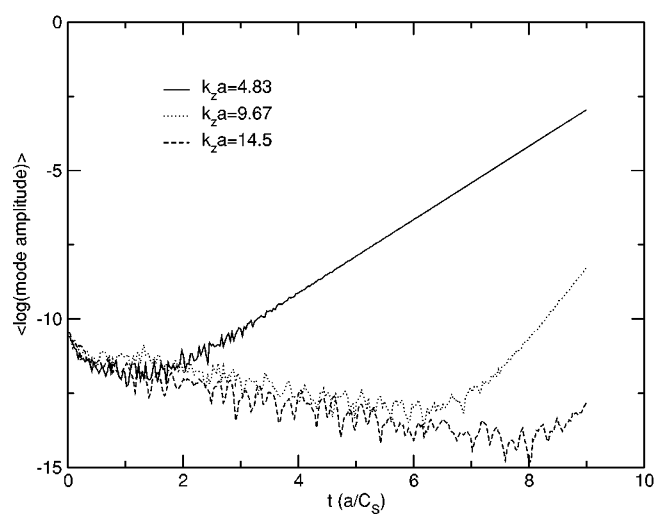

FIG. 5. Time evolution of $\langle \ln|A| \rangle$ for various wave numbers of model 1c. The growth of the mode $k_z a=9.67$ is due to nonlinear coupling.

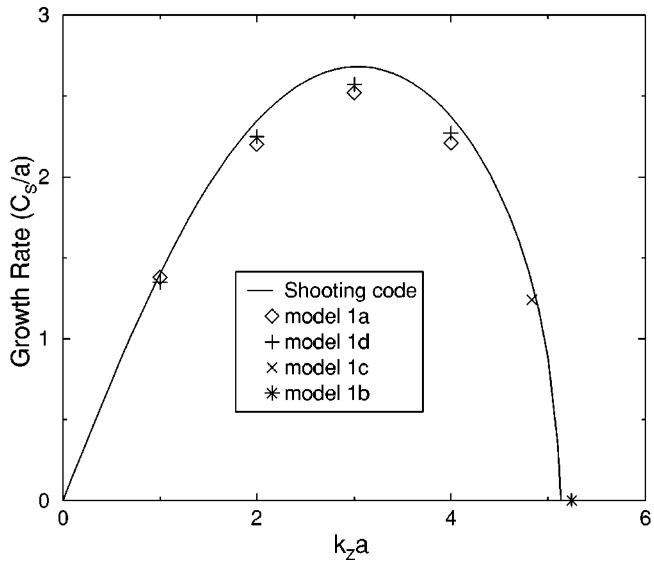

FIG. 6. A comparison of the linear growth rate obtained by simulation and by linear analysis.

more prone to the magnetic buoyancy instability. However, since elongation only slightly affects the maximum M_A, large elongation could be possible.

Another "knob" that could change the maximum M_A is the aspect ratio. From the force balance equation (11), V_A^2 scales as $aR\Omega^2$, which means M_A^2 scales as R/a. Therefore, a large aspect ratio seems to be desirable to achieve a high β system. From the magnetic buoyancy stability point of view, a large aspect ratio is also desirable. This is seen as follows. The magnetic buoyancy instability is driven by the centrifugal force $R\Omega^2$, which scales as $M_S^2 C_S^2/R$. For a centrifugally confined fusion plasma, $M_S \simeq 4$, and $T \simeq 10$ keV are required. Therefore, $M_S^2 C_S^2$ is fixed and the centrifugal force is proportional to $1/R$. For exactly the same reason, a large aspect ratio also helps the velocity shear stabilization of interchange modes, as we have shown before,[2] since the interchange mode is also driven by the centrifugal force. Figure 7 depicts the marginal stability curves for various M_S with aspect ratio $R/a=1$. When compared with Fig. 3 for $R/a=1/3$, the benefit of large aspect ratio is clearly evident. For $M_S=4$, $M_A \simeq 1.05$ can be achieved, which yields $\beta \simeq 8.3\%$.

It should be mentioned that there are two limits on the achievable M_A. The first limit is set by the MHD equilibrium: from Eq. (11), we have $M_A^2 \lesssim R/a$. The other limit is set by the MHD stability. For a high M_S centrifugal confined plasma, the schematic criterion (31) is mainly a competition between the first term and the last term of the left-hand side. Hence, the stability limit is, roughly speaking, $M_A^2 \lesssim (\pi/M_S)^2 (R/a)^2$. Since the equilibrium limit scales as R/a and the stability limit scales as $(R/a)^2$, it is possible that the latter exceeds the former in a large aspect ratio system, and the system is stable up to the equilibrium limit. For example, a $M_S=3$ system is stable to all M_A in the case $R/a=1$ (Fig. 7), whereas it is unstable at large M_A when $R/a=1/3$ (Fig. 3).

VI. SUMMARY AND DISCUSSION

In this paper, we studied the linear ideal MHD stability of a Dean flow plasma supported by an axial magnetic field. We found that the system is likely to be free of the MRI; however, the magnetic buoyancy instability could occur. The effect of aspect ratio on the MHD stability is also studied. Large aspect ratio is found to be stabilizing for the centrifugal confinement scheme. We conclude our study by discussing some issues and open questions in the present study.

(1) We considered only axisymmetric stability in this study. The primary manifestation of the MRI is two-dimensional,[6,7] as is the Parker instability.[9] Thus, our axisymmetric stability is an informative starting point. In addition, for $M_A \ll 1$, we have done a fully three-dimensional stability of the centrifuge[2,3] and found stability for large M_S. With the foregoing information, a fairly clear picture of the parameter space can be discerned. To complete this picture, however, an $M_A \sim 1$, three-dimensional stability analysis needs to be done.

(2) In this paper, we model a centrifugally confined plasma via the Dean flow model, which certainly lacks some important features. In addition to the special choices for the density, the pressure, and the flow profile, an obvious omission is the lack of the curved magnetic field, which is essential to the centrifugal confinement scheme. At first sight, curved field lines would seem more prone to the buoyancy instability. However, whether the buoyancy instability is catastrophic is not clear. It is well known in astrophysics that the plasma eventually saturates to several localized clumps after the onset of the Parker instability,[13] whereas the MRI usually results in turbulent behavior.[7] Since we have shown that the MRI will likely not destabilize the system, saturation is expected. In fact, we have run the nonlinear simulation beyond the linear growing stage. For $M_S=4$, saturation was achieved, and the final state has localized plasma clumps that in fact look like centrifugally confined plasmas. For higher M_S, the plasma was compressed to a thin disk that made running the simulation very difficult. A full discussion of this

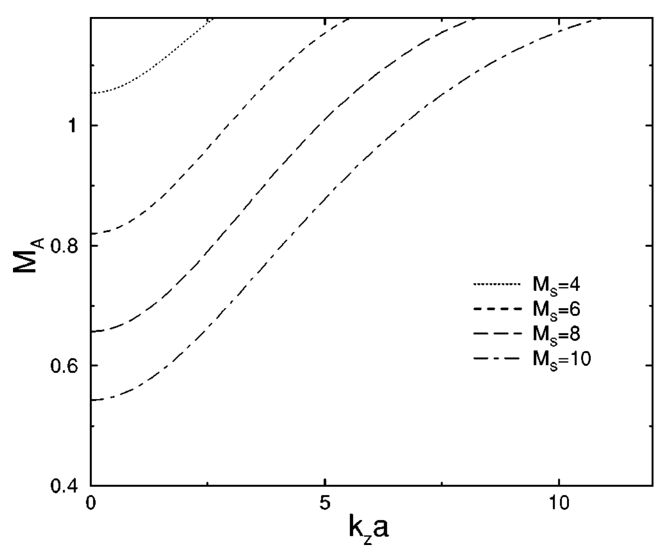

FIG. 7. Marginal stability curves for $M_S=4,6,8,10$, with $R/a=1$.

issue is beyond the scope of this paper. However, if the system indeed saturates, the buoyancy instability might not be catastrophic, and the estimate of the maximum M_{A} in the previous section may be pessimistic. It should also be mentioned that Ref. 13 assumed perfect "frozen-in" of the magnetic field. If the system is allowed to last longer than the resistive time scale, as one would expect for a steady state fusion device, then we can no longer neglect the effect of resistivity. The numerical simulation in Ref. 14 showed that on the resistive time scale, after the onset of the Parker instability, the magnetic field relaxes to a nearly uniform profile and the plasma is supported against gravity almost by the pressure gradient only. In fact, this is also what one would expect for a resistive Dean flow, even without the Parker instability. Furthermore, it is still not clear how an externally imposed curvature in the field affects the relaxation of the magnetic field. Further work is necessary to clarify the above-mentioned problems.

ACKNOWLEDGMENT

This work was supported by the DOE.

APPENDIX A: A PROOF OF THE REALITY OF ω^2 FOR THE COLD PLASMA CASE

In this appendix, we will prove the eigenvalue ω^2 to be real in the cold plasma limit as follows. First we divide Eq. (24) by $(\omega^2-k_z^2V_{\mathrm{A}}^2)\omega^2V_{\mathrm{A}}^2$, then operate the result by $\int_R^{R+a}dr\, u^*$. Integrating by parts and applying the homogeneous boundary conditions, we obtain

$$\langle|u'|^2\rangle=\left\langle\left(\frac{\omega^2}{V_{\mathrm{A}}^2}-k_z^2-\frac{3}{4r^2}-\frac{2r\Omega\Omega'}{V_{\mathrm{A}}^2}+\frac{r^2\Omega^4}{V_{\mathrm{A}}^4}-\frac{k_z^2r^2\Omega^4}{\omega^2V_{\mathrm{A}}^2}-\frac{4\omega^2\Omega^2}{V_{\mathrm{A}}^2(\omega^2-k_z^2V_{\mathrm{A}}^2)}\right)|u|^2\right\rangle, \tag{A1}$$

where $\langle\,\rangle\equiv\int_R^{R+a}dr$. The imaginary part of (A1) is

$$\mathrm{Im}(\omega^2)\left\langle\left(\frac{1}{V_{\mathrm{A}}^2}+\frac{k_z^2r^2\Omega^4}{|\omega^2|^2V_{\mathrm{A}}^2}+\frac{4\Omega^2k_z^2}{|\omega^2-k_z^2V_{\mathrm{A}}^2|^2}\right)|u|^2\right\rangle=0. \tag{A2}$$

Since the coefficient of $\mathrm{Im}(\omega^2)$ in (A2) is positive definite, we must have $\mathrm{Im}(\omega^2)=0$.

APPENDIX B: A SIMPLE DERIVATION OF THE PARKER INSTABILITY GROWTH RATE IN THE COLD PLASMA LIMIT

In this appendix, we present a simple derivation of the local Parker instability growth rate in the cold plasma limit. Suppose a cold plasma is supported against a constant gravity $\mathbf{g}=-g\hat{x}$ by a magnetic field $\mathbf{B}=B(x)\hat{z}$. The equilibrium satisfies the force balance equation

$$\frac{d}{dx}\left(\frac{B^2}{2}\right)=-\rho g. \tag{B1}$$

For small perturbations about the equilibrium, the linearized ideal MHD equations are

$$\partial_t\tilde{\rho}=-\nabla\cdot(\rho\tilde{\mathbf{u}}), \tag{B2}$$

$$\rho\partial_t\tilde{\mathbf{u}}=-\nabla(\mathbf{B}\cdot\tilde{\mathbf{B}})+\mathbf{B}\cdot\nabla\tilde{\mathbf{B}}+\tilde{\mathbf{B}}\cdot\nabla\mathbf{B}+\tilde{\rho}\mathbf{g}, \tag{B3}$$

$$\partial_t\tilde{\mathbf{B}}=\nabla\times(\tilde{\mathbf{u}}\times\mathbf{B}). \tag{B4}$$

For simplicity, we only consider two-dimensional perturbations (i.e., $\partial_y=0$). Since the system has translational symmetry along the z direction, we can assume normal modes of the form $\tilde{\rho}(x)\exp(ik_zz-i\omega t)$, etc. As we did in Sec. III B, we assume the wavelength in the z direction to be much shorter than the length scale of any fluctuation in the x direction (i.e., $\partial_x\ll k_z$).

Suppose we compress mass along a field line. This causes local density clumping according to Eq. (B2):

$$\omega\tilde{\rho}\simeq k_z\rho\tilde{u}_z, \tag{B5}$$

where $\partial_x(\rho\tilde{u}_x)$ is neglected in comparison with $k_z\rho\tilde{u}_z$, since we assume short wavelength in the z direction. As the density clumps, the extra weight causes the magnetic line to bend to balance the extra weight. This balance is Alfvénically quasistatic (i.e., $\omega\ll k_zV_{\mathrm{A}}$) and the corresponding equation is given by the x component of (B3):

$$ik_zB\tilde{B}_x\simeq\tilde{\rho}g, \tag{B6}$$

wherein the terms $i\omega\rho\tilde{u}_x$ and $\partial_x(B\tilde{B}_z)$ are neglected in view of the quasistatic and short wavelength assumptions, to be checked self-consistently later. In the presence of magnetic gradients, the field line bending results in constrictions and distensions along the flux tube. This makes matter squirt into the distended parts of the flux tube, according to the z component of (B3):

$$-i\omega\rho\tilde{u}_z=\partial_xB\tilde{B}_x=-\frac{\rho g}{B}\tilde{B}_x, \tag{B7}$$

where in the last step Eq. (B1) is used for ∂_xB. The new matter squirted into the distension makes $\tilde{\rho}$ go up even more, thus resulting in instability. The dispersion relation can be solved from Eqs. (B5) to (B7) as

$$\omega^2\simeq-\frac{g^2}{V_{\mathrm{A}}^2}. \tag{B8}$$

Notice that if g is replaced by the centrifugal force $r\Omega^2$, the local dispersion relation (26) is recovered.

To check the self-consistency of the above-mentioned derivation, we have to verify the three assumptions we have made: $\partial_x(\rho\tilde{u}_x)\ll ik_z\rho\tilde{u}_y$, $\partial_x(B\tilde{B}_y)\ll k_zB\tilde{B}_x$, and $\omega^2\ll k_z^2V_{\mathrm{A}}^2$. Now we check them in order. First of all, eliminating $\tilde{B}_x$ in Eq. (B7), using the x component of Eq. (B4), yields

$$\tilde{u}_x=-\frac{ig}{k_zV_{\mathrm{A}}^2}\tilde{u}_z, \tag{B9}$$

where we use the dispersion relation (B8) for ω^2. Hence, the assumption $\partial_x(\rho\tilde{u}_x)\ll ik_z\rho\tilde{u}_z$ requires $\partial_x(\rho\tilde{u}_x)\ll(k_z^2\rho V_A^2/g)\tilde{u}_x$, which implies

$$k_x\ll k_z^2V_{\mathrm{A}}^2/g. \tag{B10}$$

This can be satisfied as long as k_z is large enough. To check the second assumption, notice that the constraint $\nabla\cdot\tilde{\mathbf{B}}=0$ gives the relation between $\tilde{B}_x$ and $\tilde{B}_z$:

$$\partial_x \tilde{B}_x + i k_z \tilde{B}_z = 0. \tag{B11}$$

Therefore, we require $\partial_x(B\partial_x \tilde{B}_x) \ll k_z^2 B \tilde{B}_x$, which implies

$$k_x^2 \ll k_z^2. \tag{B12}$$

Again, this is consistent with the local approximation. Finally, the Alfvénically quasistatic assumption requires [using (B8)]

$$g \ll k_z V_A^2, \tag{B13}$$

which can be also satisfied in the short wavelength limit. Notice that conditions (B12) and (B13) imply condition (B10); therefore, only (B12) and (B13) are necessary. The self-consistency conditions are satisfied in the short wavelength limit; in that limit, the growth rate is independent of the wavelength. However, the above-mentioned derivation is good for $k_z a \gg 1$ [$a \sim V_A^2/g$ is the vertical length scale, from Eq. (B1)], as a result of the quasistatic approximation. If $k_z a \lesssim 1$, the Alfvénic restoring forces become more efficient (or the gravity induced clumping becomes less efficient); this causes the growth rate to drop at long wavelengths. It should also be kept in mind that all the conclusions here are only valid in the cold plasma limit. If the plasma has a nonzero temperature, the pressure will stabilize short wavelength modes. The dependence of the dispersion relation on pressure and wavelengths is the topic of the next appendix (see also Sec. III D).

APPENDIX C: LOCAL PARKER INSTABILITY GROWTH RATE: THE GENERAL CASE

In this appendix we briefly outline the derivation of the Parker instability local dispersion relation for a plasma with nonzero temperature. For simplicity we assume $p=$const and ρ=const in the equilibrium. The governing equations for a small perturbation from the equilibrium are still (B2)–(B4), except pressure has to be included in (B3):

$$\rho \partial_t \tilde{\mathbf{u}} = -\nabla(\tilde{p} + \mathbf{B}\cdot\tilde{\mathbf{B}}) + \mathbf{B}\cdot\nabla\tilde{\mathbf{B}} + \tilde{\mathbf{B}}\cdot\nabla\mathbf{B} + \tilde{\rho}\mathbf{g}, \tag{C1}$$

where $\tilde{p} = C_S^2 \tilde{\rho}$. In the following derivation we only consider perturbations with wavelengths much shorter than the characteristic length scale of the background variation such that the WKB approximation is appropriate. Under this assumption, we can assume $\tilde{\rho} \to \tilde{\rho}\exp(ik_x x + ik_z z - i\omega t)$, etc. Taking the y component of the curl of Eq. (C1) yields

$$\omega\rho(k_x \tilde{u}_z - k_z \tilde{u}_x) = k^2 B \tilde{B}_x + i k_z \tilde{\rho} g, \tag{C2}$$

where $k^2 = k_x^2 + k_z^2$. In deriving (C2) we use the constraint $\nabla\cdot\tilde{\mathbf{B}}=0$ and neglect $\tilde{B}_x \partial_x^2 B$ (which is much smaller than $k^2 B \tilde{B}_x$ by assumption) on the right-hand side. The z component of (C1) yields

$$-i\omega\rho\tilde{u}_z = -ik_z C_S^2 \tilde{\rho} - \frac{\rho g}{B}\tilde{B}_x, \tag{C3}$$

where we use (B1) for $\partial_x B$. Next, with the WKB approximation Eq. (B2) becomes

$$\omega\tilde{\rho} = \rho(k_x \tilde{u}_x + k_z \tilde{u}_z). \tag{C4}$$

Finally, the x component of Eq. (B4) is

$$-\omega\tilde{B}_x = k_z B \tilde{u}_x. \tag{C5}$$

Equations (C2)–(C5) form a closed set of variables $\tilde{u}_x$, $\tilde{u}_z$, $\tilde{\rho}$, and $\tilde{B}_x$. The local dispersion relation can therefore be obtained, after some algebra, as

$$\omega^4 - k^2(C_S^2 + V_A^2)\omega^2 + k_z^2(k^2 V_A^2 C_S^2 - g^2) = 0. \tag{C6}$$

The two solutions of ω^2 represent the fast and slow magnetosonic modes, respectively, under the effect of the gravity. The fast mode is always stable whereas the slow mode could be destabilized by the gravity; the stability criterion is

$$k^2 V_A^2 C_S^2 - g^2 > 0. \tag{C7}$$

The validity of the WKB approximation may be justified if k_x, $k_z \gg (1/B)dB/dx = g/V_A^2$. If we further assume that $C_S \ll V_A$, the dispersion relation for the slow mode can be expressed in a rather simple form:

$$\omega^2 \simeq \frac{k_z^2(k^2 C_S^2 V_A^2 - g^2)}{k^2(C_S^2 + V_A^2)}. \tag{C8}$$

Notice that in the $C_S \to 0$ and $k_x \ll k_z$ limit, the dispersion relation (B8) is recovered. As we can see from (C8), the nonzero pressure of a warm plasma stabilizes short wavelength modes. We can also apply Eq. (C7) to obtain a rough stability criterion for the Dean flow model. Recall that the Dean flow has a finite radial size a, hence $k > \pi/a$, and gravity is replaced by the centrifugal force $R\Omega^2$; the schematic stability criterion so obtained is

$$\pi^2 \frac{R^2}{a^2} > M_S^2 M_A^2, \tag{C9}$$

which is the same as what we obtained at the end of Sec. V. From Eq. (C8), for a high M_S, high M_A system (i.e. $M_S M_A \gg \pi R/a$), the "cutoff" to unstable modes occurs at $k_z^c a \sim ga/C_S V_A \sim M_S\sqrt{a/R}$, and the maximum growth rate occurs at $k_z^m a \sim \sqrt{k_z^c a}$.

[1]R. F. Ellis, A. B. Hassam, S. Messer, and B. R. Osborn, Phys. Plasmas **8**, 2057 (2001).
[2]A. B. Hassam, Phys. Plasmas **6**, 3738 (1999).
[3]Y. M. Huang and A. B. Hassam, Phys. Rev. Lett. **87**, 235002 (2001).
[4]E. P. Velikhov, Sov. Phys. JETP **9**, 995 (1959).

[5]S. Chandrasekhar, Proc. Natl. Acad. Sci. U.S.A. **46**, 253 (1960).
[6]S. A. Balbus and J. F. Hawley, Astrophys. J. **376**, 214 (1991).
[7]S. A. Balbus and J. F. Hawley, Rev. Mod. Phys. **70**, 1 (1998).
[8]A. B. Hassam, Phys. Plasmas **6**, 3772 (1999).
[9]E. N. Parker, Astrophys. J. **145**, 811 (1966).
[10]W. T. Kim and E. C. Ostriker, Astrophys. J. **540**, 372 (2000).
[11]H. T. Ji, J. Goodman, and A. Kageyama, Mon. Not. R. Astron. Soc. **325**, L1 (2001).
[12]P. N. Guzdar, J. F. Drake, D. McCarthy, A. B. Hassam, and C. S. Liu, Phys. Fluids B **5**, 3712 (1993).
[13]T. Mouschovias, Astrophys. J. **192**, 37 (1974).
[14]J. Kim, S. S. Hong, D. Ryu, and T. W. Jones, Astrophys. J. Lett. **506**, L139 (1998).